BIOMEDICAL IMAGE SUPER-RESOLUTION USING SRGAN: ENHANCING DIAGNOSTIC ACCURACY

Zübeyr Güngür [1*] (iD), İbrahim Ayaz [2] (iD), Vedat Tümen [1] (iD)

[1] *Bitlis Eren University, Computer Engineering, Bitlis, Türkiye*

[2] *Bitlis Eren University, Department of Computer Technologies, Bitlis, Türkiye*

* Corresponding Author: zubeyr1313@gmail.com

ABSTRACT

The super-resolution method, which has gained significant popularity today, aims to obtain high-resolution images from low-resolution ones, enhancing image quality and making details clearer. This technique allows for more detailed analysis of images, providing significant advantages in medical imaging, restoration of old photographs, and the analysis of security cameras. In medical imaging, super-resolution contributes to more accurate diagnosis of diseases by clarifying low-resolution MRI, CT, and ultrasound images. Similarly, in the restoration of old photographs, improving blurred visuals allows for the preservation and renewal of historically significant images. In the field of security, enhancing images obtained from low-resolution surveillance cameras makes it easier to identify suspects and allows for a more detailed analysis of events, playing a critical role in solving crimes. In recent years, deep learning-based approaches have made significant progress in the field of super-resolution. Notably, Convolutional Neural Networks (CNN) have achieved great success in solving these problems. However, one of the most remarkable developments in super-resolution is the SRGAN model, based on Generative Adversarial Networks (GAN). SRGAN has surpassed traditional methods by more effectively improving image quality. In this study, the SRGAN model was trained on three different biomedical datasets, achieving PSNR values of 31 and SSIM values of up to 94%. These results demonstrate the potential of super-resolution in enhancing biomedical imaging, offering clearer images for more accurate disease diagnosis, thereby improving the precision of medical analyses. Moreover, given that these developments can also be applied in fields such as security and restoration, the importance of super-resolution techniques across different disciplines is increasingly recognized.

Keywords: Generative adversarial networks, SRGAN, Biomedical.

1   INTRODUCTION

Super-resolution (SR) is a method of obtaining high-resolution images from one or more low-resolution versions of the same image. High-resolution images provide more detail and clarity, thereby increasing the accuracy of image analysis and classification [1]. SR technology has become increasingly important with rapid advancements in digital image processing and analysis. This technology enhances the quality and details of low-resolution images, producing high-resolution results. One of the most common problems encountered in digital images is the loss of detail and blurriness [2]. SR can address these issues by producing sharper and higher-quality images.

SR is often used to improve the quality of old or low-quality images. This technology enhances the clarity of images, providing detailed and high-quality visuals [3]. Particularly in the restoration of historically significant old photographs, SR has made a significant difference. Using SR techniques, details lost in old, low-resolution, and degraded images can be recovered, adapting the image to modern digital standards [4]. For example, enhancing and restoring the details of nostalgic and historically valuable images significantly increases visual quality, allowing these photographs to be used more effectively in modern digital formats.

One of the important application areas of SR is the medical field. In medical imaging techniques, SR enhances the resolution of images, helping doctors make more accurate diagnoses. Particularly in imaging techniques such as magnetic resonance (MR), computed tomography (CT), and ultrasound, high-resolution images allow doctors to analyze diseases in more detail [5]. The early detection of cancer cells or abnormal tissues becomes easier with SR technology, enabling the creation of more effective treatment plans for patients. Diseases identified early, especially in serious conditions like cancer, can be treated before they progress, thanks to SR.

SR also has a significant impact in the field of security and surveillance. Images obtained from security cameras are often low-resolution, and the lack of detail can result in the loss of critical information. SR technology enhances the clarity of these images, enabling the identification of suspects and the detailed analysis of events [6]. This allows security forces to intervene more effectively in incidents. Additionally, using SR technology, surveillance systems in cities can be made more efficient, and clearer results can be obtained in detecting security issues.

Super-resolution can be implemented using two main methods: Single Image Super-Resolution (SISR) and Multi-Image Super-Resolution (MISR). SISR aims to obtain a high-resolution image from a single low-resolution image [7]. This technique is often applied using deep learning models, particularly Convolutional Neural Networks (CNNs). Deep learning analyzes the features of low-resolution images and generates a high-resolution prediction. MISR, on the other hand, uses multiple low-resolution images of the same scene captured from different angles or at different times to produce a high-resolution image [8]. This method benefits from the redundancy of information across images, resulting in higher-quality outcomes.

In recent years, significant progress has been made in deep learning-based super-resolution (SR) research. Particularly, CNN-based models have demonstrated great success in addressing SR problems. CNNs are known for their strong performance in image processing and analysis and provide innovative solutions in the SR domain [9, 10]. One of the first major breakthroughs in super-resolution was the SRCNN (Super-Resolution Convolutional Neural Network) model developed by Dong et al. (2015). SRCNN uses a three-layer CNN to create high-resolution versions of low-resolution images. This model first scales a low-resolution image to a higher resolution and then performs feature extraction and reconstruction on this image [11].

After the success of SRCNN, Kim et al. introduced a deeper model called VDSR (Very Deep Super-Resolution Network). VDSR is a 20-layer deep neural network and leverages the power of deep learning to predict high-resolution versions of low-resolution images [12]. Lim et al. developed the Enhanced Deep Super-Resolution (EDSR) model, which significantly improved SR performance. EDSR uses a structure similar to VDSR but enhances performance with several key improvements [13]. The RDN (Residual Dense Network) model developed by Zhang et al. represents a new approach to SR problems and has been effective in improving resolution [14].

In deep learning-based SR research, the sharpening of blurred images has also been an important area of study in the literature. For example, Xu et al. have conducted important research in this area using deep convolutional networks to sharpen blurred images. These studies reduce blurry areas through sharpening filters, allowing fine details in the image to be emphasized [15]. Reducing random noise in digital images is important for improving image quality. Zhang et al. introduced a deep learning model called DnCNN that effectively reduces

image noise. Additionally, contrast enhancement techniques highlight the difference between light and dark areas in the image, resulting in clearer and more vibrant visuals [16].

In this study, three different biomedical datasets—skin cancer, retina fundus, and blood cell cancer—were trained with the SRGAN model [17], and the model's performance was evaluated using PSNR and SSIM metrics. The results show that for the skin cancer dataset, the model achieved a PSNR of 31.11 and an SSIM of 85.74%; for the retina fundus dataset, a PSNR of 30.75 and an SSIM of 94.83%; and for the blood cell cancer dataset, a PSNR of 33.65 and an SSIM of 88.38%. These results demonstrate the effectiveness of SR in enhancing the quality of medical images for analysis.

2 MATERIAL AND METHOD

This study uses three different datasets from global sources: the Skin Cancer dataset from the International Skin Imaging Collaboration (ISIC) [18], the Blood Cell Cancer dataset from Taleqani Hospital in Tehran, Iran [19] , and the Retina Fundus dataset from the Papageorgiou Hospital at Aristotle University of Thessaloniki [20].

2.1 Skin Cancer Dataset

From the databases of the International Skin Imaging Collaboration (ISIC), a total of 2,357 images of malignant and benign oncological diseases were obtained. These images were initially classified according to the ISIC classification and divided into equal numbers for all subsets, excluding melanomas and moles, which were slightly more prevalent. Figure 1 shows some example images from the skin cancer dataset.
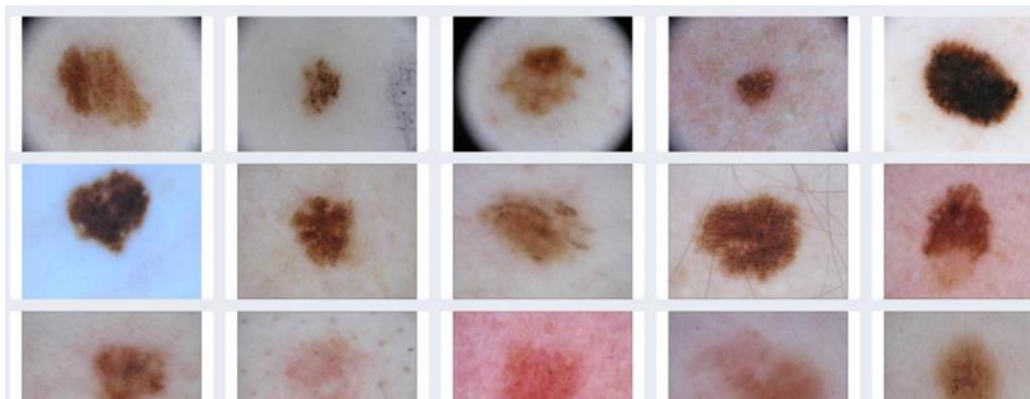

Figure 1. Skin cancer dataset sample images.

As seen in Figure 1, the dataset consists of images related to various skin lesions or moles. Irregularities in shape, color, and patterns can be observed among these lesions, which are crucial for the detection of cancerous cells [21]. The distribution of color, asymmetry, border characteristics, and size differences in the lesions are used to diagnose the disease.

2.2   Blood Cell Cancer Dataset

The accurate diagnosis of Acute Lymphoblastic Leukemia (ALL), a highly common form of cancer, often requires invasive, expensive, and time-consuming diagnostic tests [22]. Peripheral blood smear (PBS) images play a critical role in the initial screening of ALL by differentiating cancerous cells from non-cancerous cases. Manual examination of these PBS images by laboratory users is prone to diagnostic errors due to the non-specific nature of ALL's symptoms. This dataset consists of 3,242 PBS images from 89 patients suspected of having ALL, which were prepared and stained by skilled laboratory personnel. These images are divided into two classes: benign (non-cancerous) and malignant, with malignant ALL further categorized into three subtypes: Early Pre-B, Pre-B, and Pro-B ALL. All images were captured using a Zeiss camera with a 100x magnification microscope and saved as JPG files. Figure 2 shows the blood cell cancer dataset.
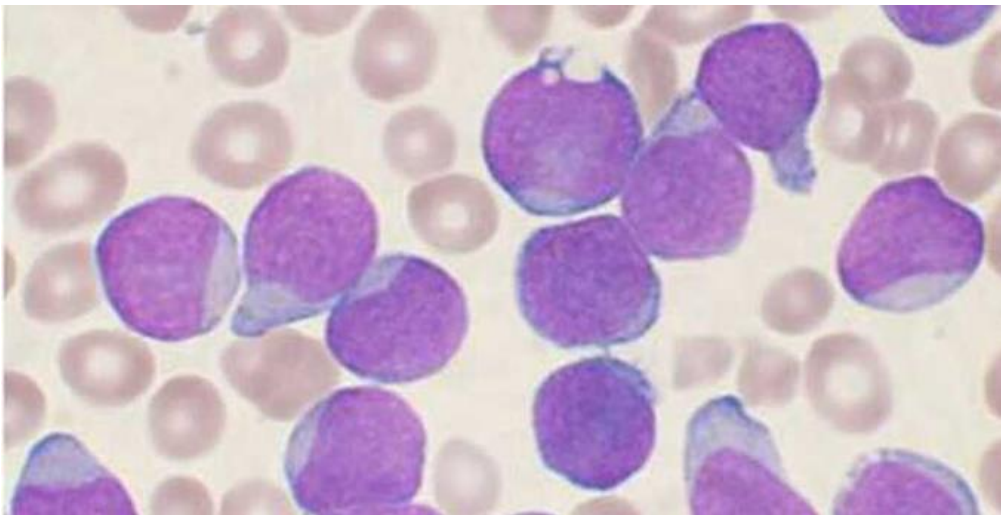

Figure 2. Blood cell cancer dataset sample images.

In Figure 2, it can be observed that cancerous blood cells are larger and have a purplish color compared to healthy blood cells. Leukemia is characterized by the uncontrolled proliferation of abnormal white blood cells in the blood and bone marrow, replacing normal cells and weakening the body's ability to fight infections and impairing other essential functions.

2.3   Retina Fundus Veri Seti

This dataset consists of 129 retinal images forming 134 image pairs, which are divided into three categories based on their features. The images were captured using a Nidek AFC-210 fundus camera with a 45° field of view. The data was collected from 39 patients at the Papageorgiou Hospital in Thessaloniki, Greece. Figure 3 shows the retina fundus dataset.
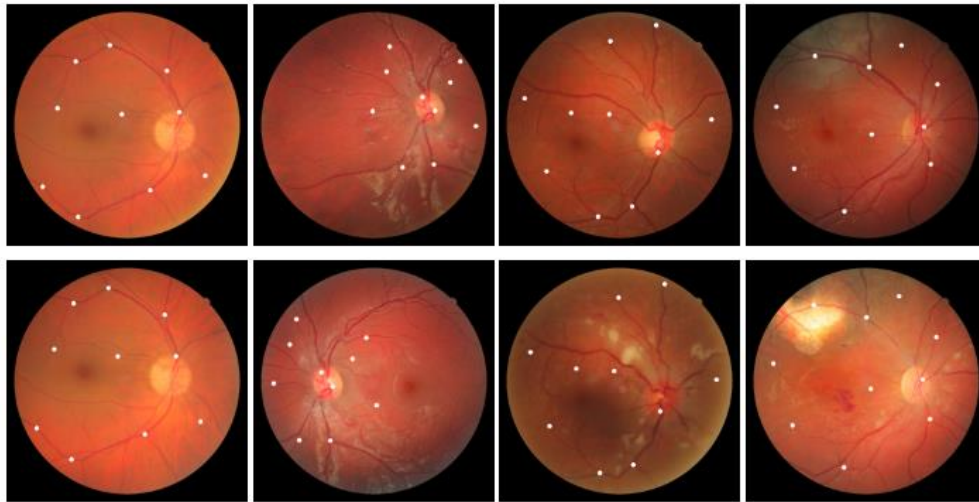

Figure 3. Retina fundus dataset sample images.

In Figure 3, the optic nerve, blood vessels, and retina surface can be seen. The optic nerve's center is usually a bright spot, and blood vessels radiate outward from this point. To diagnose eye diseases, the structure of the retinal vessels, abnormalities around the optic disc, hemorrhages, and areas such as the macula are examined. The white spots in the images are markings used to identify problem areas in the eye. Fundus images are often used to diagnose conditions such as diabetic retinopathy, where hemorrhages, cotton wool spots, and other vascular changes are significant features.

2.4   Generative Adversarial Networks

Generative Adversarial Networks (GANs) are an unsupervised deep learning framework proposed by Goodfellow et al. [23]. The framework consists of two networks: a generator (G) and a discriminator (D), optimized to minimize a two-player minimax game where the generator learns to deceive the discriminator, and the discriminator learns to protect itself from being deceived. As explained by Goodfellow and his colleagues, "The generator model can be likened to a team of counterfeiters trying to produce fake money, while the discriminator model resembles the police attempting to detect the counterfeit money" [24].

During GAN training, the generator receives a random noise vector as input and produces an output distribution PG. The discriminator is then trained to distinguish between PG and the real data distribution PData. Simultaneously, the generator is trained to learn how to deceive the discriminator. In theory, PG should converge towards PData as the discriminator becomes unable to differentiate between the generated and real samples, resulting in an ideal generator model capable of producing data following the real data distribution.

While GANs are a powerful framework, they often face stability issues, where competing networks rarely converge. Variations of the framework that use different loss functions, such as Wasserstein GANs (WGANs) [25], have been developed to improve training stability. Unlike the original GAN framework, WGANs minimize the Earth Mover's Distance and impose a gradient penalty in the loss function to constrain the discriminator's gradient norm relative to its input.

2.5   Super Resolution Generative Adversarial Networks

Super Resolution Generative Adversarial Networks (SRGAN), SRGAN is a method that uses generative adversarial networks (GANs) to produce photorealistic super-resolution (SR) images with high scaling factors. While traditional SR approaches focus on minimizing pixel-based error metrics (e.g., Mean Squared Error – MSE), SRGAN adopts an innovative perceptual loss function to produce images of a quality closer to human perception [26]. This loss function takes advantage of a discriminator network trained to distinguish between real and super-resolved images. SRGAN uses a deep residual network (ResNet) architecture and applies a VGG loss that measures the Euclidean distance between feature maps obtained from the VGG19 network. The SRGAN architecture is shown in Figure 4.
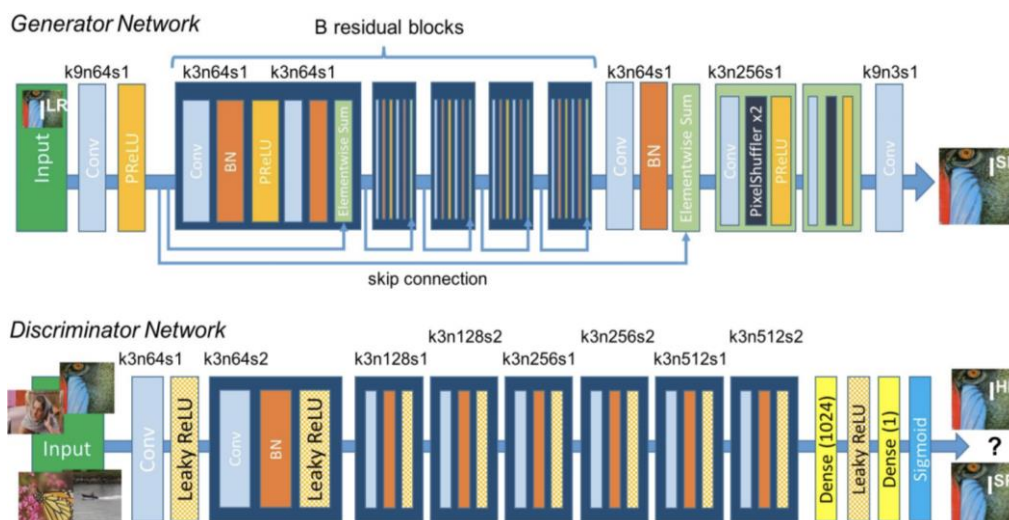

Figure 4. SRGAN Architecture.

Extensive experiments have shown that SRGAN sets a new standard for PSNR and Structural Similarity Index (SSIM) metrics on three publicly available datasets. Additionally, the quality of SR images produced by SRGAN has significantly outperformed other state-of-the-art methods, according to the results of the Mean Opinion Score (MOS) test [27]. This study demonstrates the potential of GANs in enhancing perceptual quality in the field of super-resolution.

2.6 Peak Signal-to-Noise Ratio

Peak Signal-to-Noise Ratio (PSNR) is a signal processing metric used to compare a processed signal to its original source. This comparison allows us to measure how faithfully the processed signal retains the qualities of the original, as well as to identify any noise or distortions introduced during processing [28]. PSNR directly represents the relationship between a signal before and after the degradation process. Equations 1 and 2 show these relationships.

$$PSNR = 20 \, log_{10} \frac{MAX_1^2}{MSE} \tag{1}$$

$$MSE = \frac{1}{mn} \sum_{i=0}^{m=1} \sum_{j=0}^{n=1} [(i,j) - K(i,j)]^2 \tag{2}$$

MAX is the highest possible value of the signal. In the case of an 8-bit grayscale image, AX=255, and $PSNR$ is inversely proportional to MSE (Mean Square Error), as shown in Equation (1). The final value $PSNR$ is given in decibels. PSNR is inversely proportional to MSE (Mean Squared Error), and the final value of PSNR is expressed in decibels. PSNR is commonly used to evaluate the quality of image or video signals based on the MSE relative to the source image. However, it has also been used as an analytical measure for segmentation algorithm assessments [29]. However, it has also been used as an analytical measure for segmentation algorithm assessments [30]. In the case of multi-threshold algorithms, it has been used to determine the number of thresholds in addition to their value [31].

2.6.1 Structural Similarity Index

The Structural Similarity Index (SSIM) is a metric used to evaluate the quality of digital images based on their structural integrity. SSIM was developed based on the perceptual characteristics of the Human Visual System (HVS) and, unlike traditional methods, compares the structural information of images to assess the level of degradation [32].

SSIM evaluates quality by focusing on the degradation of a scene's structural information. SSIM consists of three components: luminance, contrast, and structure. Luminance compares the average brightness values of two images; contrast is calculated based on the variance of the images; and structure is compared by calculating the covariance of the two images. The SSIM value is calculated as shown in Equation (3).

$$SSIM(x, y) = \frac{(2\mu x \mu y + C_1)(2\sigma xy + C_2)}{(\mu x_2 + \mu y_2 + C_1)(\sigma x_2 + \sigma y_2 + C_2)} \tag{3}$$

Where μx and μy are the mean brightness values of the original and distorted images, σx_2 and σy_2 are their variances, and σxy is the covariance between the two images. C_1 and C_1 are constants added for stability in the calculations.

3 RESULTS AND DISCUSSION

The PSNR and SSIM performance graphs for the skin cancer dataset after training the SRGAN model are presented in Figure 5. It is clear that during training, the PSNR value exceeds 30, which represents an ideal level for image quality [33]. Additionally, the SSIM value surpasses 85%, indicating that the generated images maintain a high level of structural integrity.
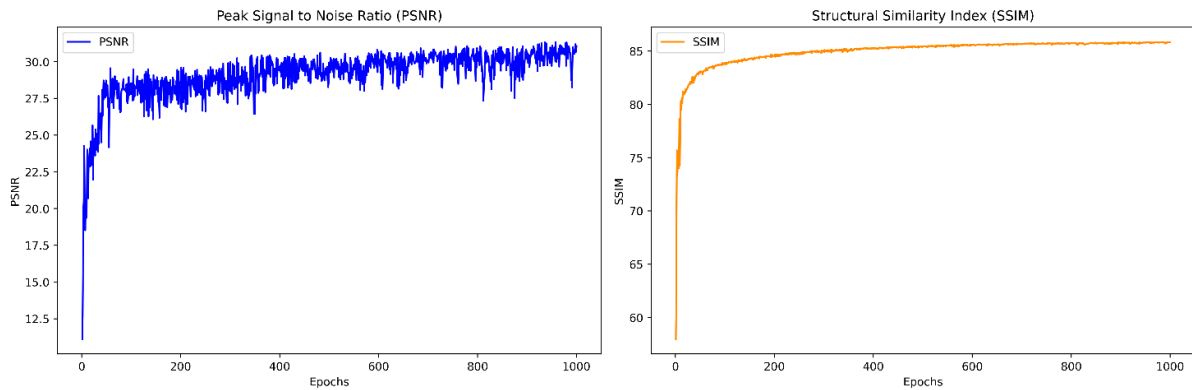

Figure 5. PSNR and SSIM Performance Graph for the Skin Cancer Dataset.

The PSNR and SSIM performance graphs for the retina fundus dataset are shown in Figure 6. During training, the PSNR value increases above 30, which is considered an excellent level for image quality [34]. Furthermore, the SSIM value approaches 95%, signifying that the generated images have a high structural resemblance to the originals.
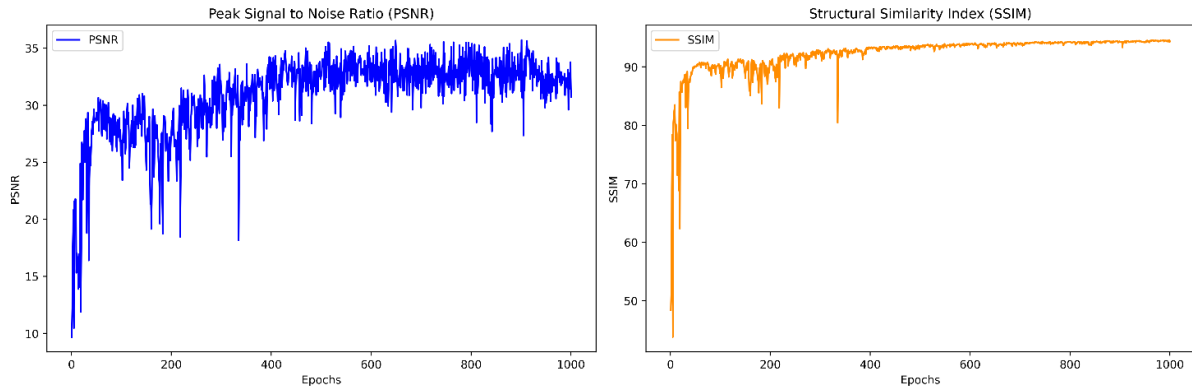
Figure 6. PSNR and SSIM Performance Graph for the Retina Fundus Dataset.

For the blood cell cancer dataset, the PSNR and SSIM performance graphs are shown in Figure 7. As illustrated, the PSNR value approaches 31 during training, and a final value of 30.97 is achieved after 1000 iterations. Additionally, the SSIM performance value of 88.18% demonstrates the structural integrity of the generated images.
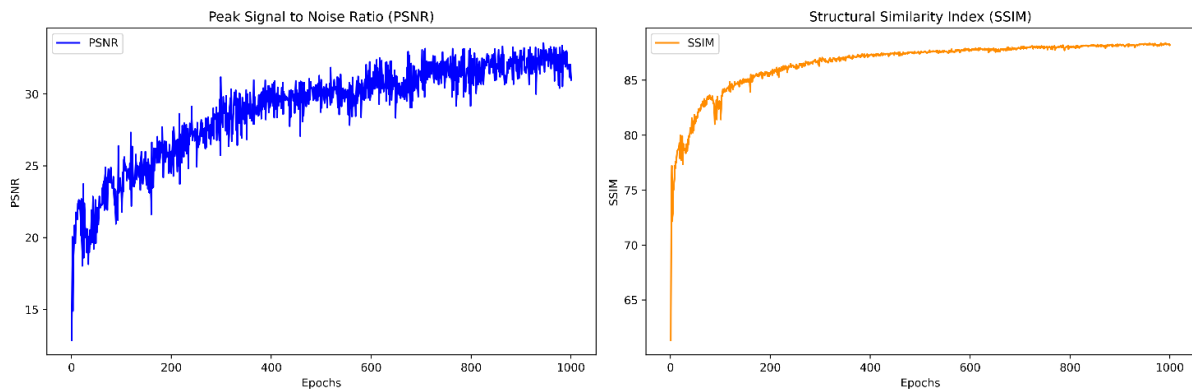

Figure 7. PSNR and SSIM Performance Graph for the Blood Cell Cancer Dataset.

The results for the SRGAN model's performance on different medical image datasets are presented in Table 1.

Table 1. Dataset Performance Values.

Datasets	PSNR	SSIM	MAE
Skin Cancer	31.06	85.84%	1.11%
Retina Fundus	30.71	94.30%	1.80%
Blood Cell Cancer	30.97	88.18%	1.51%

For the skin cancer dataset, the PSNR value of 31.06 indicates that the image quality is quite good. The SSIM value of 85.84% shows that the images have been reconstructed with high structural accuracy, while the Mean Absolute Error (MAE) value of 1.11% indicates a meager error rate. For the retina fundus dataset, the PSNR value of 30.71 represents good image

quality, and the SSIM value of 94.30% indicates an exceptionally high structural similarity to the original images. The MAE value of 1.8% shows that the model made very few errors with this dataset. Finally, for the blood cell cancer dataset, the PSNR value of 30.97 demonstrates the highest performance, indicating superior image quality compared to the other datasets. The SSIM value of 88.18% confirms the model's strong structural accuracy, and the MAE value of 1.51% indicates a low error rate. These results show that the SRGAN model can be successfully applied to different medical image datasets and effectively produces high-resolution images.

4   CONCLUSION AND SUGGESTIONS

In this study, the performance of the SRGAN model on different medical image datasets was evaluated. The results demonstrate that the model achieves successful outcomes on medical images, producing high-resolution images. Specifically, the analyses on the skin cancer, retina fundus, and blood cell cancer datasets reveal the model's overall success. Figure 8 shows the LR: Low Resolution and SR: Super Resolution images obtained as a result of the study conducted on three different original skin cancer images.
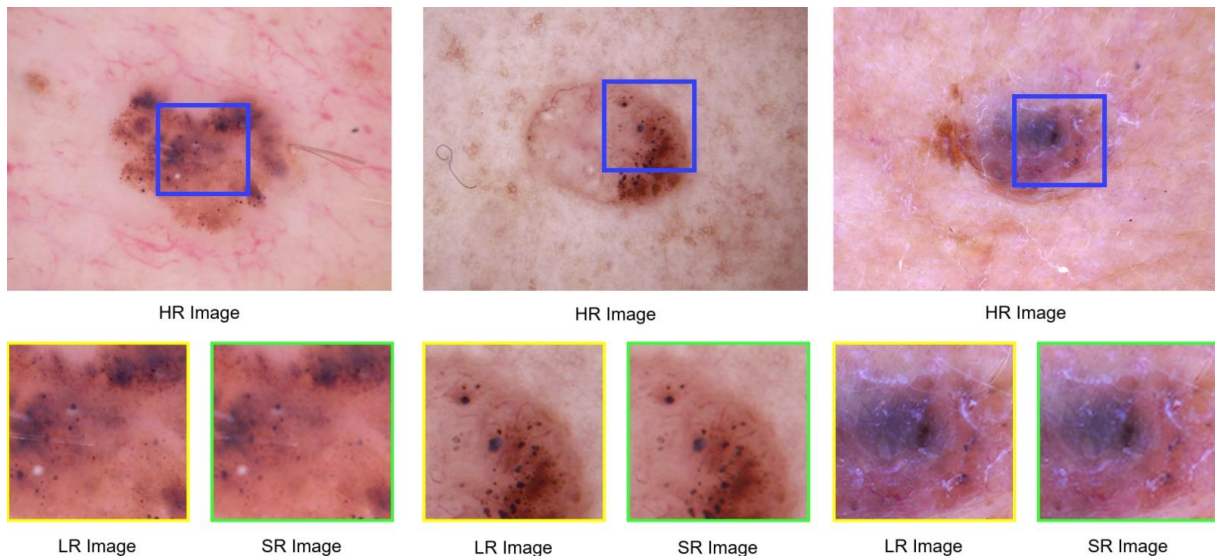

Figure 8. LR and SR results of different images in the skin cancer dataset.

For the skin cancer dataset, the PSNR value of 31.06 indicates that the image quality is quite high, which is crucial for medical diagnoses. A PSNR value above 30 suggests that the model is performing effectively. The SSIM value of 85.84% indicates that the structural integrity of the images has been preserved. The MAE value of 1.11% represents a low error rate. Figure 9 shows the LR and SR images obtained as a result of the study conducted on three different original retina fundus images.
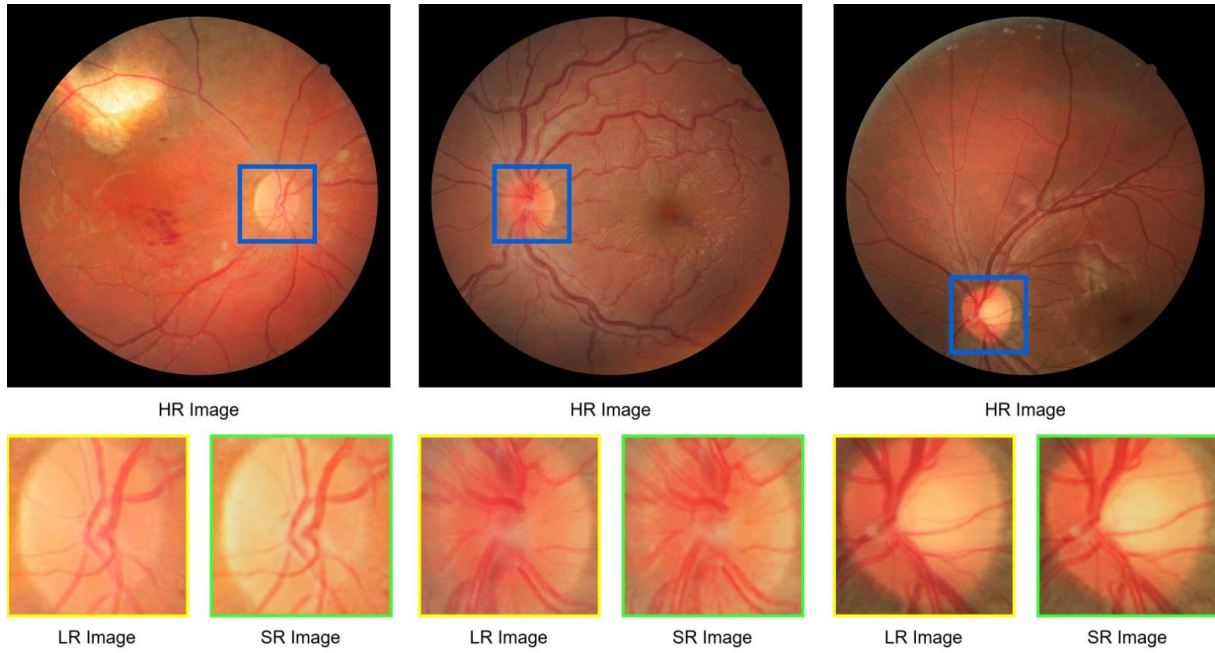
Figure 9. LR and SR results of different images in the retina fundus dataset.

For the retina fundus dataset, the PSNR value of 30.71 confirms that the image quality is high. The SSIM value of 94.30% shows a very close structural resemblance between the original and generated images. The low MAE value of 1.8% indicates that the model made very few errors on these images, suggesting that it can be applied in sensitive areas like retinal imaging. Figure 10 shows the LR and SR images obtained as a result of the study conducted on three different original blood cell cancer images.
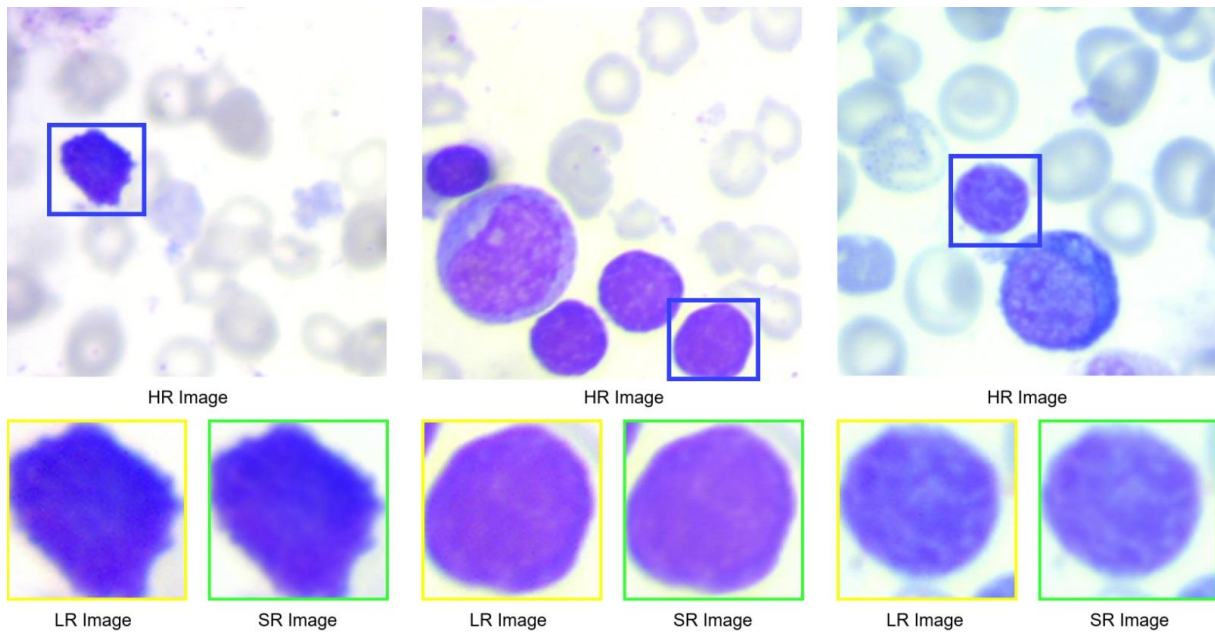

Figure 10. LR and SR results of different images in the blood cell cancer dataset.

Finally, the blood cell cancer dataset achieved the highest PSNR value of 30.97, demonstrating the best performance. The SSIM value of 88.18% confirms the model's success in maintaining structural accuracy, while the MAE value of 1.51% reflects a low error rate.

Overall, the SRGAN model has proven to generate successful results across different medical datasets. These findings indicate that the model holds great potential for medical image processing applications.

Conflict of Interest Statement

There is no conflict of interest between the authors.

Statement of Research and Publication Ethics

The study is complied with research and publication ethics.

Artificial Intelligence (AI) Contribution Statement

This manuscript was entirely written, edited, analyzed, and prepared without the assistance of any artificial intelligence (AI) tools. All content, including text, data analysis, and figures, was solely generated by the authors.

Contributions of the Authors

Zübeyr Güngür: Formal analysis; investigation; methodology; software; writing original draft; writing, review and editing.

İbrahim Ayaz: Methodology, resources, software, validation, visualization, writing original draft, writing, review and editing.

Vedat Tümen: Conceptualization, supervision, data curation, formal analysis, investigation, methodology, project administration, software, writing, review and editing.

REFERENCES

[1] P. Chopade and P. Patil, "Image super resolution scheme based on wavelet transform and its performance analysis," in *International Conference on Computing, Communication & Automation*, 2015, pp. 1182-1186: IEEE.

[2] L. Yue, H. Shen, J. Li, Q. Yuan, H. Zhang, and L. Zhang, "Image super-resolution: The techniques, applications, and future," *Signal processing,* vol. 128, pp. 389-408, 2016.

[3]   X. Hou, T. Liu, S. Wang, and L. Zhang, "Image Quality Improve by Super Resolution Generative Adversarial Networks," in *2021 2nd International Conference on Intelligent Computing and Human-Computer Interaction (ICHCI)*, 2021, pp. 117-121: IEEE.

[4]   J. Yang and T. Huang, "Image super-resolution: Historical overview and future challenges," in *Super-resolution imaging*: CRC Press, 2017, pp. 1-34.

[5]   G. Zamzmi, S. Rajaraman, and S. Antani, "Accelerating super-resolution and visual task analysis in medical images," *Applied Sciences,* vol. 10, no. 12, p. 4282, 2020.

[6]   A. Aakerberg, K. Nasrollahi, and T. B. Moeslund, "Real-world super-resolution of face-images from surveillance cameras," *IET Image Processing,* vol. 16, no. 2, pp. 442-452, 2022.

[7]   T. An, X. Zhang, C. Huo, B. Xue, L. Wang, and C. Pan, "TR-MISR: Multiimage super-resolution based on feature fusion with transformers," *IEEE Journal of Selected Topics in Applied Earth Observations and Remote Sensing,* vol. 15, pp. 1373-1388, 2022.

[8]   F. Salvetti, V. Mazzia, A. Khaliq, and M. Chiaberge, "Multi-image super resolution of remotely sensed images using residual attention deep neural networks," *Remote Sensing,* vol. 12, no. 14, p. 2207, 2020.

[9]   S. M. A. Bashir, Y. Wang, M. Khan, and Y. Niu, "A comprehensive review of deep learning-based single image super-resolution," *PeerJ Computer Science,* vol. 7, p. e621, 2021.

[10]   P. Wang, B. Bayram, and E. Sertel, "A comprehensive review on deep learning based remote sensing image super-resolution methods," *Earth-Science Reviews,* vol. 232, p. 104110, 2022.

[11]   C. Dong, C. C. Loy, K. He, and X. Tang, "Image super-resolution using deep convolutional networks," *IEEE transactions on pattern analysis and machine intelligence,* vol. 38, no. 2, pp. 295-307, 2015.

[12]   J. Kim, J. K. Lee, and K. M. Lee, "Accurate image super-resolution using very deep convolutional networks," in *Proceedings of the IEEE conference on computer vision and pattern recognition*, 2016, pp. 1646-1654.

[13]   B. Lim, S. Son, H. Kim, S. Nah, and K. Mu Lee, "Enhanced deep residual networks for single image super-resolution," in *Proceedings of the IEEE conference on computer vision and pattern recognition workshops*, 2017, pp. 136-144.

[14]   Y. Zhang, Y. Tian, Y. Kong, B. Zhong, and Y. Fu, "Residual dense network for image super-resolution," in *Proceedings of the IEEE conference on computer vision and pattern recognition*, 2018, pp. 2472-2481.

[15]   L. Xu, J. S. Ren, C. Liu, and J. Jia, "Deep convolutional neural network for image deconvolution," *Advances in neural information processing systems,* vol. 27, 2014.

[16]   K. Zhang, W. Zuo, Y. Chen, D. Meng, and L. Zhang, "Beyond a gaussian denoiser: Residual learning of deep cnn for image denoising," *IEEE transactions on image processing,* vol. 26, no. 7, pp. 3142-3155, 2017.

[17]   T. Y. Timothy, D. Ma, J. Cole, M. J. Ju, M. F. Beg, and M. V. Sarunic, "Spectral bandwidth recovery of optical coherence tomography images using deep learning," in *2021 12th International Symposium on Image and Signal Processing and Analysis (ISPA)*, 2021, pp. 67-71: IEEE.

[18]   (10.10.2024). *The International Skin Imaging Collaboration*. Available: https://www.isic-archive.com/

[19]   M. G. Mehrad Aria, Davood Bashash, Hassan Abolghasemi, and F. A. a. A. Hossein, "Acute Lymphoblastic Leukemia (ALL) image datase," ed, 2021.

[20]   C. Hernandez-Matas, X. Zabulis, A. Triantafyllou, P. Anyfanti, S. Douma, and A. A. Argyros, "FIRE: fundus image registration dataset," *Modeling and Artificial Intelligence in Ophthalmology,* vol. 1, no. 4, pp. 16-28, 2017.

[21]   R. Krithiga and P. Geetha, "Breast cancer detection, segmentation and classification on histopathology images analysis: a systematic review," *Archives of Computational Methods in Engineering,* vol. 28, no. 4, pp. 2607-2619, 2021.

[22]   C. Mondal *et al.*, "Ensemble of convolutional neural networks to diagnose acute lymphoblastic leukemia from microscopic images," *Informatics in Medicine Unlocked,* vol. 27, p. 100794, 2021.

[23]   I. Goodfellow *et al.*, "Generative adversarial nets," *Advances in neural information processing systems,* vol. 27, 2014.

[24]   I. Goodfellow *et al.*, "Generative adversarial networks," *Communications of the ACM,* vol. 63, no. 11, pp. 139-144, 2020.

[25]   M. Arjovsky, S. Chintala, and L. Bottou, "Wasserstein generative adversarial networks," in *International conference on machine learning*, 2017, pp. 214-223: PMLR.

[26]   C. Ledig *et al.*, "Photo-realistic single image super-resolution using a generative adversarial network," in *Proceedings of the IEEE conference on computer vision and pattern recognition*, 2017, pp. 4681-4690.

[27]   X. Zhu, L. Zhang, L. Zhang, X. Liu, Y. Shen, and S. Zhao, "GAN-Based Image Super-Resolution with a Novel Quality Loss," *Mathematical Problems in Engineering,* vol. 2020, no. 1, p. 5217429, 2020.

[28]   J. Korhonen and J. You, "Peak signal-to-noise ratio revisited: Is simple beautiful?," in *2012 Fourth international workshop on quality of multimedia experience*, 2012, pp. 37-38: IEEE.

[29]   Y.-K. Chen, F.-C. Cheng, and P. Tsai, "A gray-level clustering reduction algorithm with the least PSNR," *Expert Systems with Applications,* vol. 38, no. 8, pp. 10183-10187, 2011.

[30]   M.-H. Horng and R.-J. Liou, "Multilevel minimum cross entropy threshold selection based on the firefly algorithm," *Expert Systems with Applications,* vol. 38, no. 12, pp. 14805-14811, 2011.

[31]   S. Arora, J. Acharya, A. Verma, and P. K. Panigrahi, "Multilevel thresholding for image segmentation through a fast statistical recursive algorithm," *Pattern Recognition Letters,* vol. 29, no. 2, pp. 119-125, 2008.

[32]   Z. Wang, A. C. Bovik, H. R. Sheikh, and E. P. Simoncelli, "Image quality assessment: from error visibility to structural similarity," *IEEE transactions on image processing,* vol. 13, no. 4, pp. 600-612, 2004.

[33]   D. R. I. M. Setiadi, "PSNR vs SSIM: imperceptibility quality assessment for image steganography," *Multimedia Tools and Applications,* vol. 80, no. 6, pp. 8423-8444, 2021.

[34]   U. Sara, M. Akter, and M. S. Uddin, "Image quality assessment through FSIM, SSIM, MSE and PSNR—a comparative study," *Journal of Computer and Communications,* vol. 7, no. 3, pp. 8-18, 2019.